Temporal Modeling of High Frequency (30 - 100 kHz) Acoustic Seafloor Backscatter: Shallow Water Results.

D. D. Sternlicht and C. de Moustier

Marine Physical Laboratory
Scripps Institution of Oceanography
9500 Gilman Drive
La Jolla, CA 92093-0205, USA
E-mail: dan@mpl.ucsd.edu

Abstract

A temporal model of high frequency seafloor acoustic backscatter is presented and compared to recorded echoes from terrigenous sediments. Using acoustic properties correlated with mean grain size, the echo shapes and amplitudes of the model are compared to data collected in San Diego Harbor with fully calibrated 33 kHz and 93 kHz narrow beam piston transducers. While there is considerable variation for small horizontal translations of the transducer, the mean echo envelopes compare well with the shapes and amplitudes predicted by model simulations.

1. Introduction

In recent years a number of acoustic techniques have been developed for characterizing the upper layer of seafloor sediment: [1, 2, 3, 4, 5, 6]. While empirical techniques have demonstrated market value, we are investigating a physical approach with a temporal model of high frequency acoustic seafloor backscatter. Using geo-acoustic parameters correlated with the grain-size distribution of ocean sediments, this model simulates the shape and magnitude of echo-envelopes received by a monostatic transducer aimed at the bottom. The primary goal in working with a temporal representation is to facilitate a greater understanding of acoustic scattering at the bottom/sub-bottom interface. However, the ability to match simulations with measured echo envelopes, where the only unknowns are the bottom characteristics, is the foundation of a sediment classification tool currently under development.

The *temporal model* predicts average echo shapes and energy levels for realistic scenarios defined by acoustic frequency, sediment type, system configuration, and deployment geometry. The software representation of the model was developed by iterative comparisons to data recorded with a fully characterized system. In this paper we first describe the mathematical formulation of the model. Specifications and calibration of a dual frequency system are then presented along with the signal processing steps necessary after echo digitization. Deployment of the system and data collection are described, followed by comparisons of the model with recorded echoes from fine-grade, shallow water sediments, where the transducers were inclined 0 to 16 degrees from nadir. Finally, we discuss the prospects of using the temporal model as a tool for sediment classification.

2. Model

The *temporal model* simulates the expected intensity envelope of echo-sounding monostatic piston transducers operating between 10 and 100 kHz. It incorporates the transducer's geometry and beam pattern, ocean volume spreading and absorption losses, and the geoacoustic parameters which describe the water/bottom interface and the sediment volume. The model component representing interface backscatter incorporates the roughness spectrum of the interface, the local bottom slope, and a coherent reflection coefficient. Sediment volume backscatter is derived from the spectrum of subbottom refraction index fluctuations, and the roughness characteristics of the interface governing sound transmission to the sediment.

Figure 1 illustrates the process described by the model. A short acoustic pulse represented by the arc, insonifies

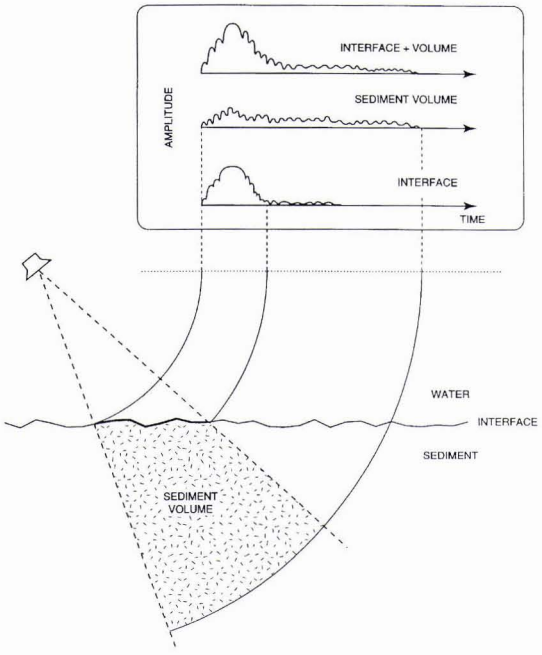

Figure 1: Graphic representation: Temporal Model of High Frequency Acoustic Seafloor Backscatter

the sediment which scatters energy back to the transducer. The graphs in the upper right corner depict the measured backscatter from the insonified areas and volumes as a function of time. The bottom graph represents the backscatter from the sediment/water interface as the projection of the pulse onto the seafloor traverses the main lobe of the transducer. The middle graph represents energy penetrating the sediment volume and scattering from subbottom inhomogeneities. The model computes these components separately and combines them to estimate the measured signal represented by the top graph.

Consider a transducer which insonifies the bottom with a short, non-uniform pulse, and subsequently measures the echo. $I(t)$ is the integral over the bottom area and represents the backscattered energy coincident upon the transducer face at time t:

$$I(t) = \int_A \frac{(I_i + I_v)\, b(\phi, \psi)}{r^2\, 10^{\alpha_w(\frac{r}{10})}} dA$$

In this formulation, A is the area of seafloor which has come into contact with the transmitted pulse; b represent the directivity, where ϕ and ψ are angles referencing the transducer axes and elemental area, dA; r is the distance between the transducer and dA; and α_w is the seawater absorption coefficient. I_i and I_v represent the interface and sediment volume backscatter intensities referenced 1 meter from dA. I_i is the product of transmitted intensity incident at dA and interface backscatter function $\sigma_i(\rho, \nu, \gamma, \omega_2, f_a, \theta)$. σ_i is based on the Kirchhoff approximation as described in Jackson et al [7] and Mourad and Jackson [8], where; ρ and ν are the relative density and the relative sound-speed; γ and ω_2 are the exponent and strength of the roughness spectrum, f_a is the acoustic frequency of the pulse, and θ is the incidence angle of the wave-front upon the interface. With slight modification to Jackson et al, I_v is calculated by integrating the subbottom component of the signal, the sediment attenuation α_v, and the sediment volume backscatter function σ_v through the sediment, and properly modulating by the interface roughness statistics governing transmission through the interface.

For most natural seafloor surfaces, the variance of heights between two points on the seafloor increases as the distance between the points, l, becomes larger. In our measurements l represents the horizontal distance traveled by the pulse within the transducer's footprint - where the footprint, $l_f = 2\, alt\, \tan(\theta_{bw}/2)$, is defined at normal incidence by the transducer's half power beam width θ_{bw}, and altitude over the bottom, alt. For situations where the variance of sea-floor heights is large compared to the transmitted pulse length, the output of the temporal model may be convolved with the corresponding altitude distribution as described in Pouliquen [4]. When applying

this method, we assume that the altitude is normally distributed with variance equal to the structure function described in [7] and evaluated with l: $\sigma_h^2 = D_h(l)$.

3. System

For testing the *temporal model* we built a dual-frequency echosounder system which was calibrated in a shallow water tank. A Hewlett Packard Arbitrary Wave Form Generator creates a gated sinusoid which is amplified by an ENI 2100 power amplifier. The TR (Transmit-Receive) switch constructed for this system has 2 input channels (power amplifier and A/D) and one output to the transducer. Its active circuit allows the high-voltage output signal to excite the piezoelectric ceramic transducer, while protecting the receive circuitry. The small transducer voltages generated by the echo, pass undistorted through the TR switch and are subsequently amplified, band pass filtered, and digitized by a Gagescope CS125 oscilloscope card, sampling slightly faster than the outgoing signal's Nyquist frequency. An Applied Geomechanics clinometer, measuring pitch and roll at 0.1 degree resolution, is installed parallel with the transducer face and sampled every ping repetition. Envelope detection is performed by inverse system filtering (described in section 3.2), base-banding, and low pass filtering.

3.1. Transducer Specifications

For each transducer, the following table summarizes the acoustic transmit frequency (f_a), half power beam width (θ_{bw}), transmit pulse length (τ_p), transmit voltage response (TVR in dB re: 1 μPa/Volt @ 1 m), and the open circuit voltage response (OCV in dB re: 1 Volt/μPa).

Transducer	f_a (kHz)	θ_{bw} (deg)	τ_p (msec)	TVR (dB)	OCV (dB)
Reson TC2084	33	21	0.450	164.5	-179.0
AirMar M192	93	10	0.160	157.5	-176.5

The measured beam patterns of these transducers are conical, approximated by the first order Bessel function, with sidelobes lower than -15 dB.

3.2. Extracting Pressure Signal from Voltage Time Series

To exploit the angular dependence of seafloor acoustic backscatter, short acoustic pulses are used to insonify a series of small sectors within the footprint. This ideal scenario is illustrated by the arcs of figure 1. The footprint becomes smaller with decreasing altitude, therefore the pulse must be made commensurately smaller. However, the shortest pulse length achievable is roughly $1/\Delta f$, where Δf is the transducer bandwidth. In this work we operate with pulse lengths close to this limit and correct for the rise/fall times introduced by the device's transfer function.

In its raw form, the *temporal model* assumes a uniform frequency response for the transducer, but few transducers have such ideal characteristics - especially when operated near resonance. Thus we must convert the measured voltage waveforms into the correct pressure waveforms before comparison with the model. The transducer's mechanical-electrical transfer function is determined by deconvolving a direct path measurement, made with an independent broadband hydrophone, from the signal received by the transducer after reflection from a flat aluminum plate. Figures 2.a and 2.b show the digitized direct path and reflection measurements, $x(t)$ and $y(t)$, while figure 2.c shows the corresponding spectra. Figure 2.d presents the mechanical-electrical transfer function, $H(f)$, calculated as $H(f) = Y(f)/X(f)$.

The input to the temporal model of seafloor acoustic backscatter is thus, the echo envelope of the direct path measurement, appropriately scaled using the TVR. The output of the temporal model is compared to measured echoes which have been inverse filtered ($H^{-1}(f)$) and appropriately scaled using the OCV.

4. Measurements

The difficulty of reproducing representative seafloor substrates and appropriately scaled survey geometries in the lab, makes field testing of the model mandatory. Development of the model was therefore coordinated with echoes measured pier-side and underway from a small launch.

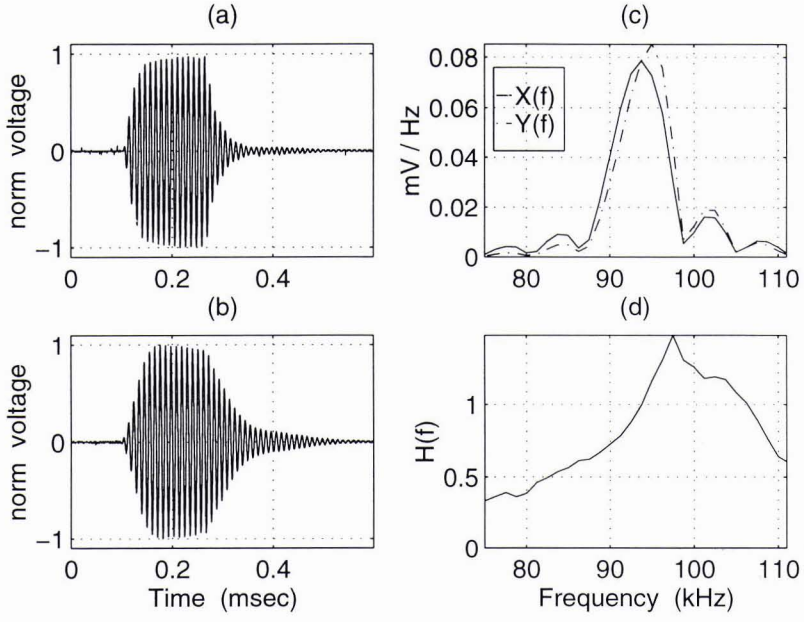

Figure 2: AirMar M192 signal characteristics @ 93 kHz: (a) $x(t)$, transmit signal; (b) $y(t)$, reflected signal; (c) $X(f)$ and $Y(f)$, spectra; (d) $H(f)$, transfer function

4.1. Pier-side Measurements

Preliminary versions of the model were compared to measurements from a transducer attached firmly to a pier insonifying a flat section of seafloor. These tests confirmed the accuracy of the time-base and relative sound intensity levels predicted by the model, and demonstrated the necessity of incorporating the transducer's transfer function in shallow water applications. In sequences of pings recorded over 5 minute intervals, echo shapes were nearly identical. Thus, the acoustic character of the bottom below the pier varies slowly over time, yielding stable echo statistics. In addition similar bottom stability is expected during the 20 minutes of a short survey in the bay, such that variability in the echo structure should be mostly due to changes in substrate roughness or composition.

4.2. Shallow Water Survey

In January of 1997, the echo sounder described in section 3 was installed in the instrument well of the 40 foot launch ECOS, operated by NRaD. We surveyed a N-S trackline of the San Diego Harbor trough - the deepest part of the bay with depths of 15-20 meters. With survey speeds of 1-2 knots and ping repetition rate of 5 Hz, the bottom was typically sampled 30 to 60 times over the length of a footprint. Bottom echoes were recorded with the 33 kHz and 93 kHz transducers inclined 0 to 16 degrees from nadir in the roll plane. Angles of pitch and roll were digitized for each ping repetition. Sea conditions were mild, with pitch and roll standard deviations typically less than 0.5 degrees.

4.3. Survey Site Bottom ID

Bottom characterization was based on video coverage recorded during the survey, consulting a sediment data base for the surrounding area, and the analysis of particle size distribution for several sediment grabs taken during the survey. The *Mean Grain Size*, M_ϕ, of the samples is calculated via Inman [9]. This standard method for characterizing sediments assumes that the variable $\phi = -log_2(D_g)$, where D_g is the measured grain size in mm, is normally distributed. Analysis of the samples implies that the substrate ranges between *Clayey Sand* and *Sandy Mud* per the labeling scheme set forth in the *High-Frequency Ocean Environmental Acoustic Models Handbook* [10]. Associated with these sediments are empirically derived values of the geoacoustic parameters used in the sediment interface and volume backscatter functions and summarized in the following table:

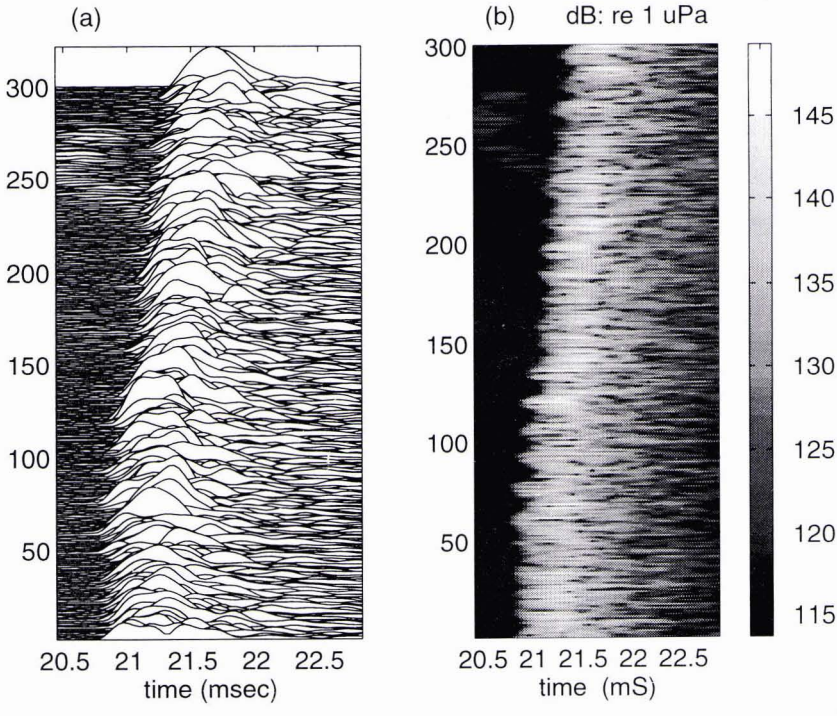

Figure 3: Survey Data - 33 kHz

Site	Sed Name	M_ϕ	ρ	ν	σ_2	γ	ω_2 (cm^4)
North	Clayey Sand	4.093	1.224	1.0364	0.002	3.25	0.001119
South	Sandy Mud	5.876	1.149	0.9873	0.001	3.25	0.000518

These values are defined in section 2, where σ_2 is known as the *volume parameter* and defined by $\sigma_2 = \sigma_v/\alpha_v$.

The video image reveals an uncomplicated bottom, appearing as long stretches of homogeneous substrate. This, combined with $> 98\%$ spatial overlap of echoes and the generally level bathymetry, were conditions we felt ideal for testing the accuracy of the temporal model.

4.4. Data

The *waterfall plot* of figure 3.a displays 300 consecutive bottom echoes received with the 33 kHz transducer. These measurements were made underway, with the transducer inclined 2 degrees with respect to nadir in the roll plane. Figure 3.b displays the same data in raster grayscale format expressed in dB re: 1 μPa. The abscissa represents time after pulse transmission. Using the standard approximation of sound speed in seawater (1500 m/sec), the transducer's altitude over the bottom is $\sim$16 meters, the footprint diameter is $\sim$6 meters and, at 5 Hz ping repetition, spatial overlap amounts to $\sim$60 pings per footprint diameter. The raster image for this 40 second (20 meter) track segment shows the gradual downward slope of the bottom modulated by the vessel heave. The early returns evident in pings 230-280 are, most likely, caused by a school of fish swimming over the bottom.

4.5. Ping Alignment and Averaging

The waterfall plot demonstrates the high variability of echo amplitude and shape for horizontal translations which are small compared to the diameter of a footprint. The scattering theory employed is stochastic, and upon averaging echo envelopes, the form and amplitude predicted by the temporal model takes shape. Before averaging, pings

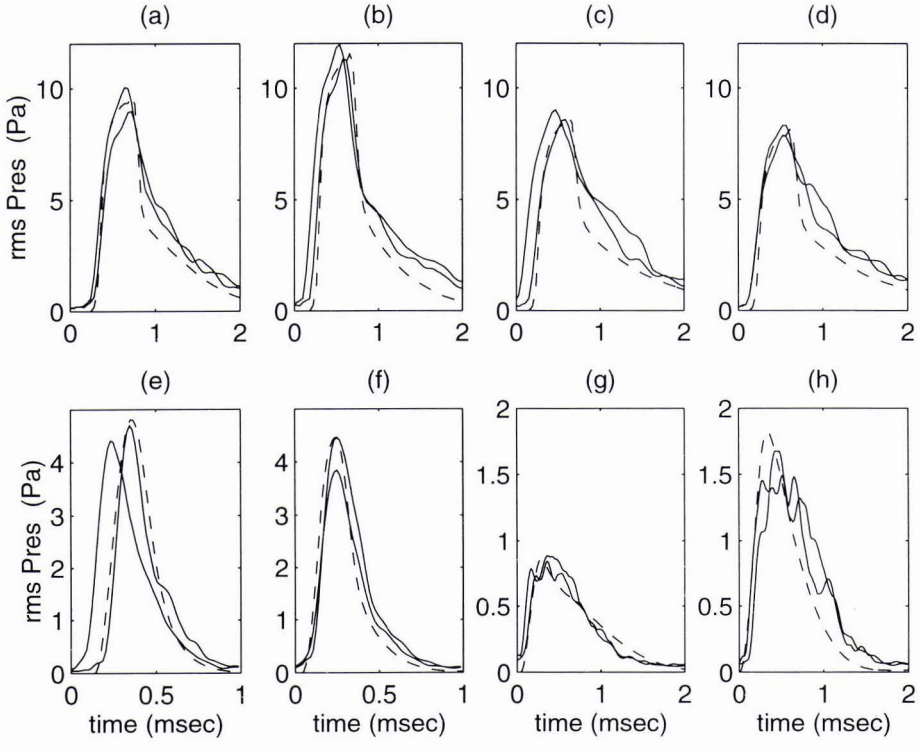

Figure 4: Model vs Data

are aligned along a minimum amplitude threshold, filtering out vessel heave and small fluctuations in altitude. Pressure envelopes are averaged using a kernel of 20 pings, discounting sections of data in which fish or vegetation are obviously present.

4.6. Analysis

Figure 4 compares the *temporal model* with data for scenarios where the main lobe of the transducer intersects the bottom near-normal and slightly off-normal, as summarized in the following table:

	$f_a(kHz)$	θ_T (deg)	alt (m)	M_ϕ	d_s (cm)	σ_h (cm)	$macro$
(a)	33	2.0	15.63	5.0	64	2.9	
(b)			15.80	4.5	38	3.6	
(c)		8.0	16.35	4.3	39	5.2	
(d)			16.40	4.5	38	4.8	
(e)	93	2.0	19.35	4.2	14	3.1	√
(f)			19.27	5.0	23	2.2	√
(g)		8.5	18.97	6.0	74	2.7	√
(h)			18.82	4.0	15	4.0	√

where the acoustic frequency (f_a), transducer tilt angle (θ_T), and altitude (alt) are preset, or directly measured quantities; and the mean grain size (M_ϕ) represents the descriptive parameter used to generate the model. The quantity (d_s) represents the calculated 10 dB skin depth of the inferred substrate - taking into account the sediment

absorption and the interface transmission coefficients, and σ_h represents the standard deviation of the altitude due to macro-roughness. Note that due to the gentle slope of the bottom in this area, θ_T approximates the main lobe's incidence angle with the seafloor.

For these graphs, the theoretical pressure envelope, $P(t)$, is derived from the square root of the modeled intensity envelope, $I(t)$: $P(t) = [I(t) \cdot \rho_w \cdot c_w]^{1/2}$, where c_w and ρ_w denote respectively the sound speed and the density of seawater. Dashed lines represent the model output for mean grain size (M_ϕ) values between 4 and 6. Solid lines represent aligned/averaged data. The graphs are arranged such that pairs (a,b), (c,d), (e,f), (g,h) represent data from the same track - where each graph shows two averaged envelopes displayed approximately 50 pings apart. While data and model are displayed with the time-base shifted to zero, their relative temporal positions remain intact.

From inspection of the graphs, the *temporal model* does a reasonable job predicting the mean amplitude of the data, where measured amplitudes appear to obey Gaussian or Rayleigh statistics, and amplitudes near-normal are larger than off-normal - due to the angular dependence of the backscatter functions. Also evident from the graphs is the agreement in echo shape between model and data. The echoes for the off-normal measurements are longer than those measured near normal incidence as the tilted transducer insonifies a longer swath of the bottom. We expect that matches in amplitude and shape, as functions of M_ϕ and θ_T, will be useful tools in identifying seafloor substrates.

For most natural sediments, the variance of heights (σ_h^2) over a given footprint (l_f) increases as the mean grain size increases. Sediments dominated by large grains are considered to be *rougher* than sediments dominated by small grains. This relationship can be seen in (σ_h) for the data pairs of figure 4. The most dramatic example is the 1.3 cm increase in (σ_h) between data pair g and h, as the inferred substrate changes from *sandy mud* to *clayey sand*. The 33 kHz and 93 kHz transmit signals have physical round-trip lengths in water of 34 cm and 12 cm respectively. On comparing these lengths with σ_h, we applied the macro-roughness convolution described at the end of section 2, to model calculations for the 93 kHz transducer. As a result, the modeled returns appear smoother, thus simulating the effect of averaging echoes from a substrate with relatively large σ_h.

While the data shown here are well-behaved, there are segments of data which exhibit energy spurs, ocurring after the expected interface return, and not predicted by the volume component. This may be due to large scale roughness or to the presence of a subbottom layer. Inspection of skin depth (d_s) implies that for appreciable backscatter to occur, this layer would have to exist within a meter of the sediment/water interface for the finer sediments, and within 50 cm for the substrates with M_ϕ nearly equal to 4 - as dictated by the difference in sediment absorption coefficient between *sandy mud* and *clayey sand*. From these observations we infer that small changes in the large scale interface roughness are responsible for the variation in shape and amplitude observed in the data.

5. Conclusions

In this paper we have described a temporal model of high frequency acoustic seafloor backscatter, demonstrating ability to estimate the shape and amplitude of stacked/averaged echoes collected under survey conditions. In shallow water applications, the accurate representation of signal and data are important for making meaningful comparisons. Therefore in this procedure, the transducer's directivity, transmit/receive response, and mechanical-electrical transfer function are used for expressing model and data in physical units, and to insure fidelity in signal shape.

The appropriate choice of variables for calculating large scale interface roughness (macro-roughness) and sediment volume backscatter is not entirely clear, and better understanding of these issues should increase the model's accuracy. Furthermore, we need to investigate a more robust method of calculating representative echo envelopes from the raw data - as in better methods of stacking, averaging, and filtering. With echo shape and backscatter strengths derived from model and data, we are currently working on algorithms which compare these features and deduce sediment type.

Acknowledgements

We thank NRaD, ENI Inc., Reson Inc., and MPL's DeepTow staff for their technical support, and we thank ONR for supporting this work under Contract # N00014-94-1-0121.

References

[1] T. K. Stanton and C. S. Clay, "Sonar echo statistics as a remote sensing tool: Volume and Seafloor", *IEEE Transactions of Ocean Engineering*, vol. OE-11, No. 1, pp. 79-96, 1986.

[2] S. G. Schock and L. R. Le Blanc and L. A. Mayer, "Chirp Subbottom Profiler for quantitative sediment analysis", *Geophysics*, vol. 54, pp. 445-450, 1989.

[3] R. Chivers and N. Emerson and D. R. Burns, "New acoustic processing for underway surveying", *The Hydrographic Journal*, No. 56, pp. 9-17, 1990.

[4] E. Pouliquen, "Identification des fonds marins superficiels a l'aide de signaux d'echo-sounders", Doctoral Thesis, Univ. Paris VII, 1992.

[5] D. R. Jackson and K. B. Briggs and K. L. Williams and M. D. Richardson, "Test of models for high-frequency seafloor backscatter", *IEEE Journal of Oceanic Engineering*, vol. 21, No. 4, pp. 458-470, 1996.

[6] S. J. Dijkstra and L. A. Mayer, "Lassoo!: An interactive graphical tool for seafloor classification", *Proceedings of OCEANS 89*, pp. 1064-1070, 1996.

[7] D. R. Jackson and D. P. Winebrenner and A. Ishimaru, "Application of the composite roughness model to high-frequency bottom backscattering", *Journal of the Acoustical Society of America*, vol. 79, pp. 1410-1422, 1986.

[8] P. D. Mourad and D. R. Jackson, "High frequency sonar equation models for bottom backscattering and forward loss", *Proceedings of OCEANS 89*, pp. 1168-1175, 1989.

[9] D. L. Inman, "Measure for describing the size distribution of sediments", *Journal of Sedimentary Petrology*, vol. 22, pp. 125-145, 1952.

[10] Applied Physics Laboratory - University of Washington, "High-Frequency Ocean Environmental Acoustic Models Handbook", Technical Report APL-UW TR 9407 AEAS 9501, October 1994.